

## Article

# Copper Wire Resistance Corrosion Test for Assessing Copper Compatibility of E-Thermal Fluids for Battery Electric Vehicles (BEVs)

Bernardo Tormos <sup>1</sup>, Santiago Ruiz <sup>1</sup>, Jorge Alvis-Sanchez <sup>1,\*</sup> and Leonardo Israel Farfan-Cabrera <sup>2</sup>

<sup>1</sup> Clean Mobility & Thermofluids, Universitat Politècnica de València, 46022 Valencia, Spain; betormos@mot.upv.es (B.T.); saruiz@mot.upv.es (S.R.)

<sup>2</sup> Escuela de Ingeniería y Ciencias, Tecnológico de Monterrey, Monterrey 64849, Mexico; farfanl@tec.mx

\* Correspondence: jalvsan@mot.upv.es

**Abstract:** This study aims to assess the compatibility of various e-thermal fluids for immersion cooling in battery electric vehicles through a copper wire resistance corrosion test. The tested fluids include a polyalphaolefin, diester, mineral oil API G-III, transformer oil, and a fully formulated dielectric coolant. The test was conducted at 130 °C for 336 h, and the resistance of the copper wires was monitored in vapor and oil phases. By comparing the resistance variation and analyzing portions of the wires through scanning electron microscopy, it was found that the vapor phase of PAO and diester in one of the tests exhibited significant corrosion, while the dielectric coolant showed minimal corrosive effects, implying better compatibility. These results provide insights into the corrosion behavior and compatibility of the fluids with copper, which are essential for selecting suitable dielectric fluids for immersion cooling applications in electric vehicles.

**Keywords:** battery thermal management; immersion cooling; e-thermal fluid; copper; corrosion; resistance; oxidation; copper wire resistance corrosion test; copper compatibility



**Citation:** Tormos, B.; Ruiz, S.; Alvis-Sanchez, J.; Farfan-Cabrera, L.I. Copper Wire Resistance Corrosion Test for Assessing Copper Compatibility of E-Thermal Fluids for Battery Electric Vehicles (BEVs). *Batteries* **2024**, *10*, 285. <https://doi.org/10.3390/batteries10080285>

Academic Editors: James Marco and Carlos Ziebert

Received: 24 April 2024

Revised: 4 July 2024

Accepted: 7 August 2024

Published: 9 August 2024



**Copyright:** © 2024 by the authors. Licensee MDPI, Basel, Switzerland. This article is an open access article distributed under the terms and conditions of the Creative Commons Attribution (CC BY) license (<https://creativecommons.org/licenses/by/4.0/>).

## 1. Introduction

The electrification of the transport sector worldwide is paving the way for battery electric vehicles (BEVs) to become a prominent part of the modern automotive landscape. As many countries have set ambitious targets for the incorporation of these vehicles, this has led to 10 million electric cars being sold globally in 2022, which is an increase of 52% from the previous year [1]. With this rapid expansion arrives new challenges, particularly in terms of battery thermal management (BTM). Issues such as battery overheating during charging and discharging pose risks to efficiency, longevity, and safety, including potential concerns related to thermal runaway [2]. One promising solution for addressing such challenges is immersion cooling, a form of direct liquid cooling that involves submerging the battery cells in a dielectric fluid to extract heat from the cells. Applications of this method also include the cooling of electronic devices such as computer servers, data centers, and power transformers, as well as batteries [3].

The main advantage of such cooling systems when compared to air cooling or indirect liquid cooling is their significantly higher rate of heat removal, which is particularly important for effectively managing thermal loads of high-capacity batteries (enabling fast charging) [3]. This allows the battery temperature to be maintained at its optimal level, improving efficiency, extending lifetime, and ensuring safe operation by preventing thermal runaway [4]. The cooling fluid must have electrically insulating (dielectric) properties to prevent the short circuiting of the battery, as well as ideal thermal properties for removing heat [3]. A fluid with these characteristics is known as an e-thermal fluid. For these cooling systems, selecting an appropriate dielectric fluid is critical to preventing adverse effects on the immersed components, particularly copper components, which are commonly found in electric applications.

While assessing various aspects of potential e-thermal fluids, material compatibility holds significant importance, primarily owing to the anticipated extended lifespan of these fluids (fill for life) [5]. Consequently, conducting compatibility assessment tests becomes imperative, and with copper being the primary conductor of electricity in this application, both the fluid and the copper materials must not negatively affect one another.

The assessment of fluid compatibility with copper materials highlights the significance of standardized tests such as the ASTM D130 standard [6]. Although this standard serves as a benchmark for evaluating the copper compatibility of lubricants through a well-established procedure, it might not give enough information about the corrosion process. To fill this gap, there are emerging methodologies that have not been standardized yet, such as the conductive deposit test and the copper wire resistance corrosion test (CWRCT).

The CWRCT has been previously employed to assess copper corrosion in the context of lubricants for traditional and electrified transmissions [7,8], providing insights into the compatibility of various fluids with copper components. This method has been used to evaluate the corrosion rates of lubricants, revealing insights into the kinetics and mechanisms of copper corrosion across various temperatures [9]. These investigations underscored the CWRCT's sensitivity and efficiency, enabling real-time assessments that are crucial for formulating lubricants that safeguard against corrosion under operational conditions. Furthermore, this method presents attractive potential for evaluating next-generation immersion cooling fluids for BEVs. Hence, immersion cooling can be key to redefining thermal management in EVs. However, ensuring the compatibility of immersion cooling fluids with copper components becomes paramount. The methodology established for the CWRCT could be used to analyze the interaction between these advanced dielectric fluids and copper, which is vital for optimizing battery performance and longevity. This adaptation could bridge the gap between traditional corrosion assessment techniques and the evolving needs of thermal management solutions in the electric mobility sector, as highlighted by advancements in fluid formulations.

In this paper, the copper compatibility of several thermal fluids was tested by conducting accelerated experiments with two different heating methods for different thermal fluids. One consisted of using heating plates while the other consisted of using a thermal bath. The corrosion of copper through the tests was monitored and acquired by measuring the resistivity through the entire immersion period.

By analyzing the interaction between these dielectric fluids and copper, this research aims to provide a different approach to understanding copper compatibility that will help optimize e-thermal fluid formulation and, therefore, battery performance and longevity, bridging the gap between traditional corrosion assessment techniques and the evolving needs of thermal management solutions in the electric mobility sector. The structure of the article is as follows: Section 2 details the materials and methods employed in the study, including the experimental setup, fluid selection, and testing procedures. Section 3 presents the results and discussion, analyzing the resistance measurements, scanning electron microscopy (SEM) observations, and copper debris quantification. Finally, Section 4 concludes the study, summarizing the findings and their implications for the development of immersion cooling systems for BEVs.

## 2. Materials and Methods

The experimental setup (Figure 1) consisted of placing 500 mL of each test fluid in a 1 L beaker. A 1 m length and 42 American Wire Gauge-caliber (63.5  $\mu\text{m}$  in diameter) pure-copper wire (99.9%) was submerged in each fluid, while another wire was placed above the fluid to evaluate both oil and vapor phases.

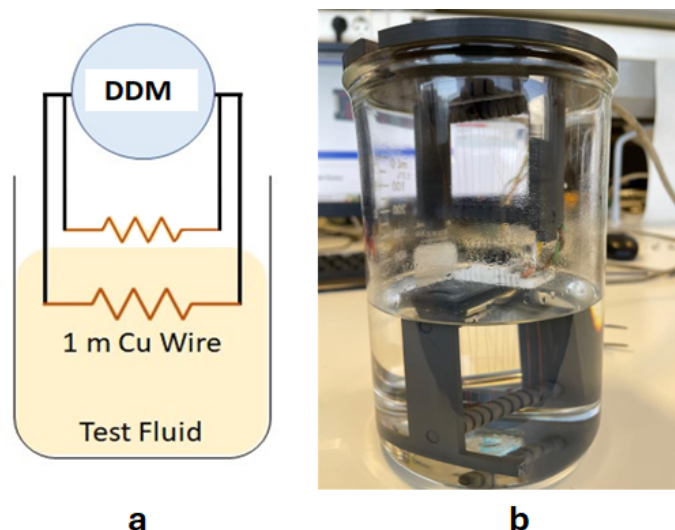


**Figure 1.** Copper wire corrosion resistance test (CWRCT) set-up. (a) schematic diagram, (b) photograph of the final set-up.

Commercially available copper wires come in different presentations with different coatings, which need to be removed to expose the surface that will be in contact with the fluid's environment. In this experiment, the selected wire had an enamel coating that was carefully removed using formic acid as a solvent. Figure 2 shows the diameters before and after removing the enamel coating of a wire. The diameters of all the tested wires oscillated between 60 and 60.8  $\mu\text{m}$  after coating removal. It is noteworthy that the coating removal process perhaps also attacked the copper surface, also removing part of the copper surface.

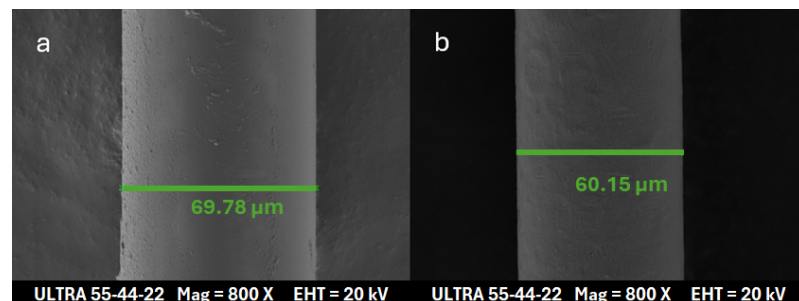


**Figure 2.** SEM images obtained from the tested copper wire: (a) diameter measurement of the copper wire with enamel coating; (b) diameter measurement of the copper wire without enamel coating.

The immersion tests were conducted at a working temperature of 130 °C ( $\pm 1$  °C) for 336 h. A digital data multimeter (DDM) was employed to measure the resistance of the copper wires with a 1 mA direct current through the entire immersion period.

Despite surpassing the optimal operational range of a battery pack (around 25 °C) [10,11], heating the fluid at 130 °C is vital in this experiment. The objective is to observe the long-term effects of immersion cooling in BEV between copper and the working fluid; thus, elevated temperatures facilitate oxidation for both the fluid and the copper wire [12–15]. This process of oxidizing copper (along with any other possible reaction) will reduce the amount of copper capable of conducting electricity; consequently, an increase in resistance is expected. Although products of copper oxidation might also be conductive or semi-conductive, they are far less conductive than pure copper [16,17]. Hence, resistance is considered the indicator of the corrosiveness of the fluid on copper due to the removal of the material, since the resistance of a wire is provided by the following formula [18]:

$$R = \rho \frac{4L}{\pi d^2} \quad (1)$$

where  $R$  is the resistance of the wire,  $\rho$  is the resistivity of copper,  $L$  is the length of the wire, and  $d$  is the diameter of the wire. Hence, it is assumed that if the copper wire is corroded by the fluid, the wire's cross-sectional area will decrease, increasing the overall resistance. Resistance measurements were taken using the 4-wire resistance method (or Kelvin method) for higher accuracy [19]. Table 1 shows the accuracy of the equipment used for the tests.

**Table 1.** Accuracy of equipment employed.

Equipment	Variable Measured/Controlled	Accuracy
Thermal bath	Temperature	$\pm 0.25\text{ }^{\circ}\text{C}$
Heating plates	Temperature	$\pm 0.5\text{ }^{\circ}\text{C}$
DDM	Resistance	$\pm 57.8\text{ m}\Omega$
ICP	Concentration	$\pm 1\text{ ppm}$

The thermal fluids tested using the CWRCT were as follows: a polyalphaolefin (PAO4)-based oil, API G-III hydrocarbon-based oil, a synthetic-ester-based oil (Diester), a transformer oil, and a fully formulated dielectric coolant. Each fluid was tested twice to evaluate the repeatability of the results. Table 2 indicates a description of these test fluids and the corresponding heating method, and Table 3 shows some of their general properties. The two different heating methods are illustrated in Figure 3.

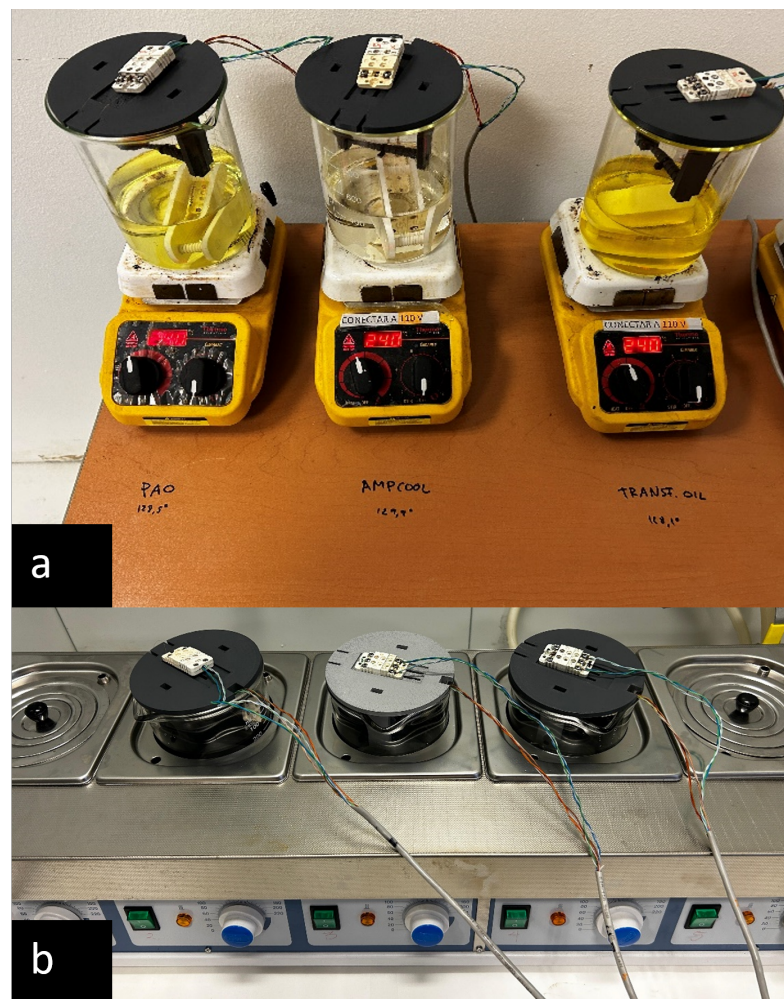


**Figure 3.** CWRCT setup with different heating methods: (a) heating plates; (b) thermal bath.

**Table 2.** Fluids and heating method description.

Heating Method	Fluid	Notation	Type
Heating plates (HP), Thermal bath (TB)	PAO4	PAO	Base stock Polyalphaolefin (API G-IV)
Thermal bath (TB)	DIESTER	DE	Base stock synthetic Ester (API G-V)
Thermal bath (TB)	G-III	G-III	Base stock mineral oil (API G-III)
Heating plates (HP)	TRANSFORMER OIL	TR	Fully formulated mineral transformer oil
Heating plates (HP)	DIELECTRIC COOLANT	DC	Fully formulated biodegradable synthetic hydrocarbon

**Table 3.** Fluid properties.

Fluid	Density @20 °C (kg/m <sup>3</sup> )	K. Viscosity @100 °C (cSt)	Thermal Conductivity @20 °C (W/m K)	S. Heat Capacity @20 °C (kJ/kg K)	Flash Point (°C)
PAO	816	4.03	0.145	2.314	204
DE	913	3.25	0.146	2.076	220
G-III	828	4.29	0.138	2.210	198
TR	852	5.91	0.135	2.184	187
DC	823	2.20	0.137	2.127	190

After the immersion period (336 h) of each test, the wires were removed and cleaned to be observed via SEM. This was carried out in order to analyze the possible degradation damage that occurred to the wires. Simultaneously, an inductively coupled plasma mass spectrometry (ICP) test was performed on three samples of each fluid to detect the possible copper concentration dissolved.

### 3. Results and Discussion

#### 3.1. Resistance Measurements

Resistance measurements in the CWRCT are mainly focused on detecting changes caused by oxidation due to exposure to the test fluids. This is the most likely scenario that would significantly alter the resistance of the copper wire during the test. While other factors can affect resistance, the controlled conditions of the CWRCT minimize their impact. Temperature is maintained at a constant throughout the test, eliminating thermal effects [20] (excluding the temperature variation during the day and night in the heating plates tests). The use of direct current avoids frequency-related resistance changes [21]. The isolated wire configuration and low current level (1 mA) make proximity effects [22] and induced magnetic fields negligible. Although mechanical stress can affect resistance, the wires are carefully placed to minimize tension, and any additional stress would likely cause rupture before significantly affecting resistance due to the area- and length-dependent nature of the relationship (Equation (1)). Finally, the high purity of the copper wire (99.9%) ensures that impurities are not a contributing factor to resistance changes [23], leaving oxidation as the primary focus of the CWRCT.

As a reference, the resistance of an additional clean wire exposed at room temperature (23 °C) was measured simultaneously through an additional CWRCT, as shown in Figure 4. The comparison of the resistances, given for a wire diameter of 60 µm, are shown in Table 4. Throughout the whole test, the average resistance of the control copper wire did not substantially change, staying at an average of 6.101 Ω with no more than 2% standard deviation due to room-temperature changes; therefore, no significant corrosion was produced.

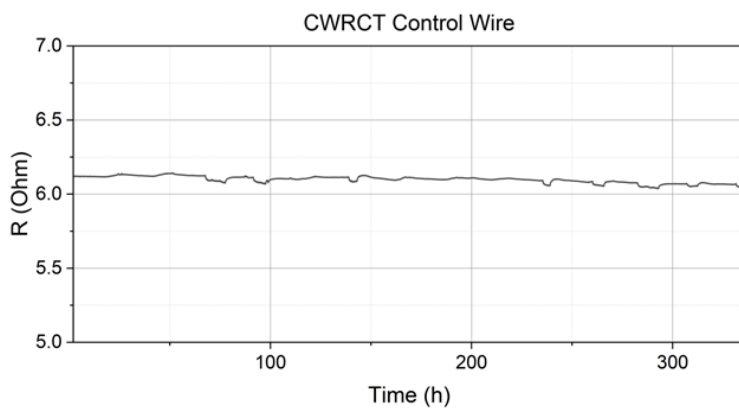


**Figure 4.** Resistance measurement of the control wire.

**Table 4.** Comparison of theoretical and experimental resistances obtained for a 60  $\mu\text{m}$  diameter.

Method	R ( $\Omega$ )
Theoretical (calculated using Equation (1))	6.0974
Experimental (measured)	6.1012

Initial resistance values in each test might differ due to different factors, such as temperature, length, and uncertainties in the DDM connections. Additionally, due to the configuration of the test, where one wire is submerged in the fluid while the other one is placed above, the temperature of the oil phase will be higher than that of the vapor phase since temperature control is achieved with the oil phase; this temperature difference displays a resistance difference in all tests due to the relationship between them [20]:

$$R(T) = R_0[1 + \alpha(T - T_0)] \quad (2)$$

where  $R(T)$  is the resistance at temperature  $T$ ,  $R_0$  is the resistance of the wire at a reference temperature,  $T_0$  (typically room temperature), and  $\alpha$  is the temperature coefficient of resistance.

Figures 5 and 6 show the results obtained via the tests performed with heating plates as the heating method. In Figure 5, the first resistance measurement data using the heating plates showed that the wire in the PAO vapor phase failed after 140 h, while the rest increased their resistance by less than 1.5%. The second test did not exhibit the same failure of the PAO\_VAP or any evidence of severe damage, since the resistance measurements did not increase by more than 1.5% in all wires.

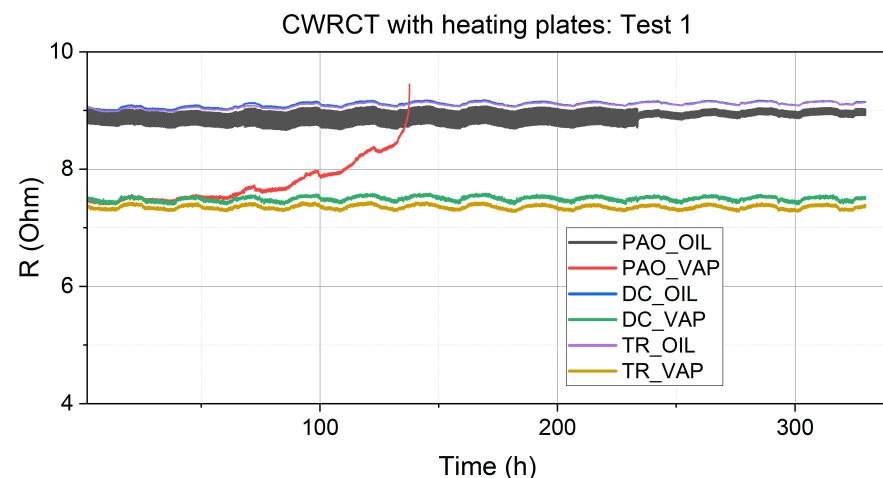


**Figure 5.** Resistance with immersion time for the different fluids using heating plates; test 1.

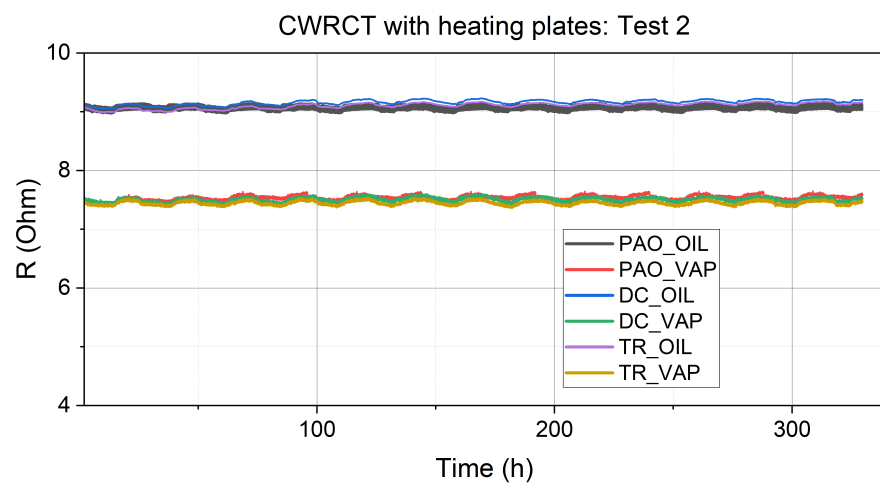


**Figure 6.** Resistance with immersion time for the different fluids using heating plates; test 2.

Oscillations observed in the resistance measurements appeared as a consequence of the high fluctuations in ambient temperature between day and night, taking into account that heating plates were used to control temperature; therefore, there was a higher difference in resistance between the vapor and oil liquid phases. Figure 7 shows the comparison of resistance changes in both repeated tests (and difference between them) using heating plates.

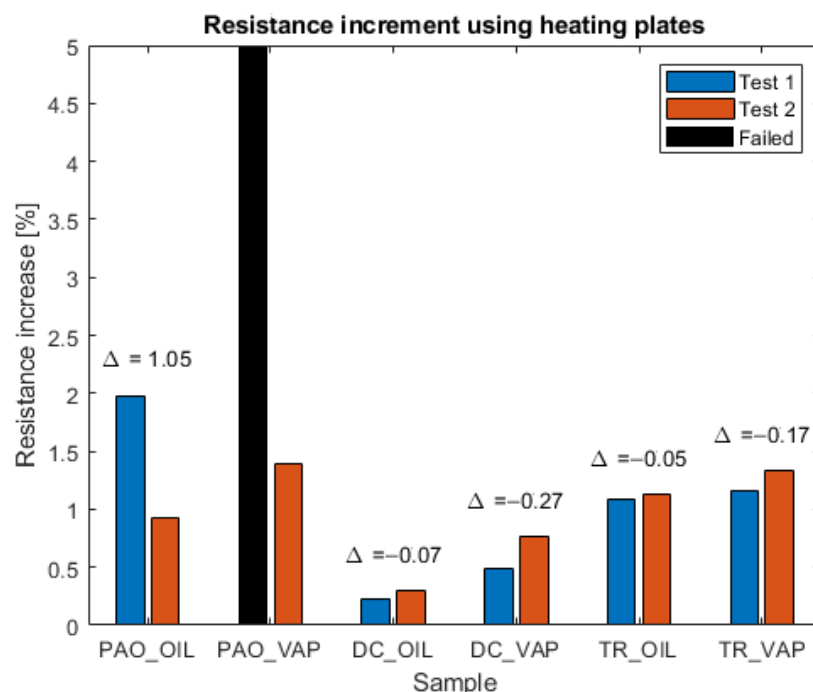


**Figure 7.** Comparison of resistance changes obtained from the two tests using heating plates.

The resistance results obtained via the measurements conducted using a thermal bath for heating are shown in Figures 8 and 9. Each figure shows the results of one test repeat. Overall, all the results show more stable resistance behavior than those obtained by using the hot plates (See Figures 5 and 6). This is because using the thermal bath ensured uniform temperature control in the oil phase and prevented higher heat losses compared to the heating plates' arrangement. Therefore higher resistance values were measured in this setup and no oscillations were observed.

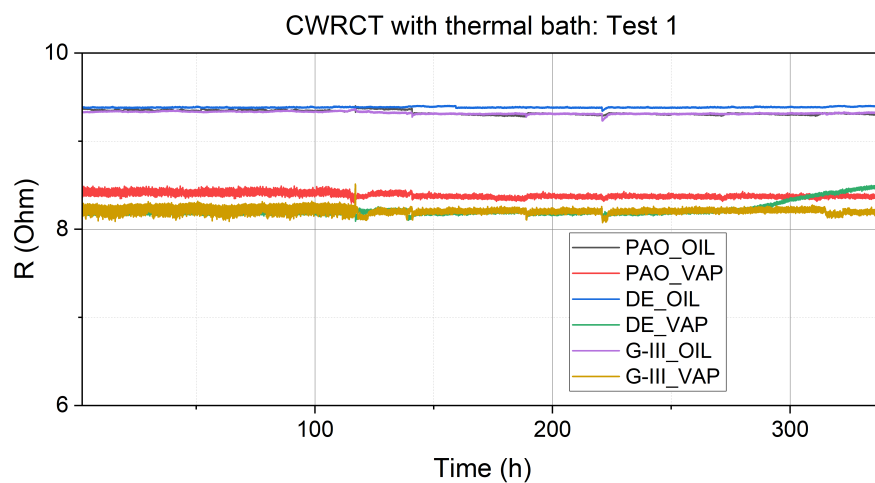


**Figure 8.** Resistance with immersion time measurements for the different fluids using the thermal bath for heating; test 1.

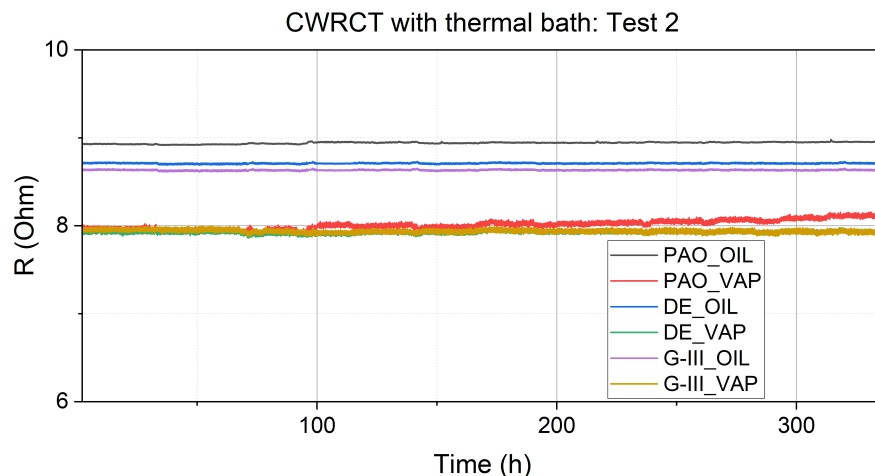


**Figure 9.** Resistance with immersion time measurements for the different fluids using the thermal bath for heating; test 2.

In an initial test (Figure 8), the wire exposed to the vapor phase of the diester showed a steady linear increase in resistance after 270 h, while the other wires did not show more than a 1% increase (Figure 9).

The second test performed with the thermal bath showed that the wire exposed to the PAO in the vapor phase increased by 2.67% at the end of 336 h, with a linear increase starting at around 100 h, as shown in Figure 9. Figure 10 shows the resistance changes in both tests (and the difference between them) in the thermal bath setup.

Although most wires did not exhibit a substantial increase in resistance over the course of the experiments, the most affected ones were those in the vapor phase. When a wire failure occurred, the presence of green droplets around the wire was observed (Figure 11). This phenomenon is often indicative of the generation of copper (II) hydroxide  $\text{Cu}(\text{OH})_2$  as a corrosion byproduct from the reaction with oxygen and moisture present in the air [24–27].

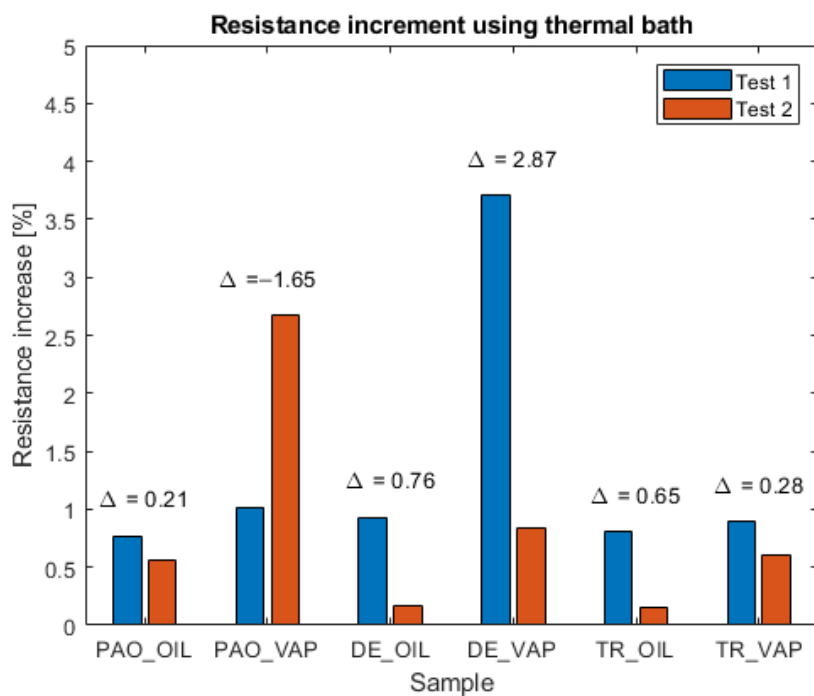


**Figure 10.** Comparison of resistance changes obtained from two tests using a thermal bath.

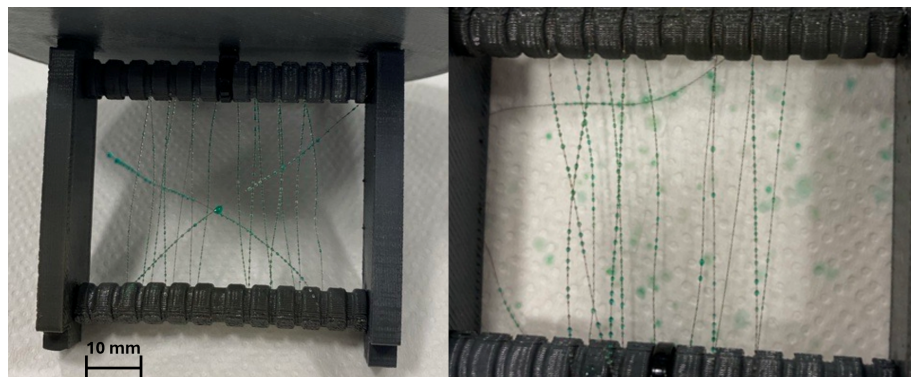
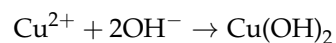
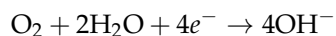


**Figure 11.** Green  $\text{Cu}(\text{OH})_2$  droplets found in the most affected wires in the PAO vapor phase.

In the reaction, copper needs to form  $\text{Cu}^{2+}$  ions, which will combine with hydroxide ( $\text{OH}^-$ ) ions from the reduction of oxygen to form copper(II) hydroxide as follows:



When combined, the overall balanced chemical equation is as follows:



### 3.2. Scanning Electron Microscope Analysis

Portions of the wires were observed via SEM to analyze the effects of corrosion and quantify the elements detected on the surface. Table 5 shows an elemental analysis of the surface of the wire and the percentage of elements found in all tests.

The wires most affected by corrosion were those exposed to the vapor phase of the PAO (heating plates 1), DE (thermal bath 1), and PAO (thermal bath 2). They showed a significant decrease in copper found on the surface and elevated amounts of oxygen, which indicates a higher concentration of copper oxides. Furthermore, the remaining wires exhibited a smaller decrease in copper from 92.33% to 55% and 73% and a minor increase in oxygen, moving from 0.06% up to 10%. Additionally, carbon was also found in concentrations higher than 20%, possibly indicating remains from the fluids (hydrocarbons) and debris/contamination from the environment. Figure 12 presents images of the three most affected wires.

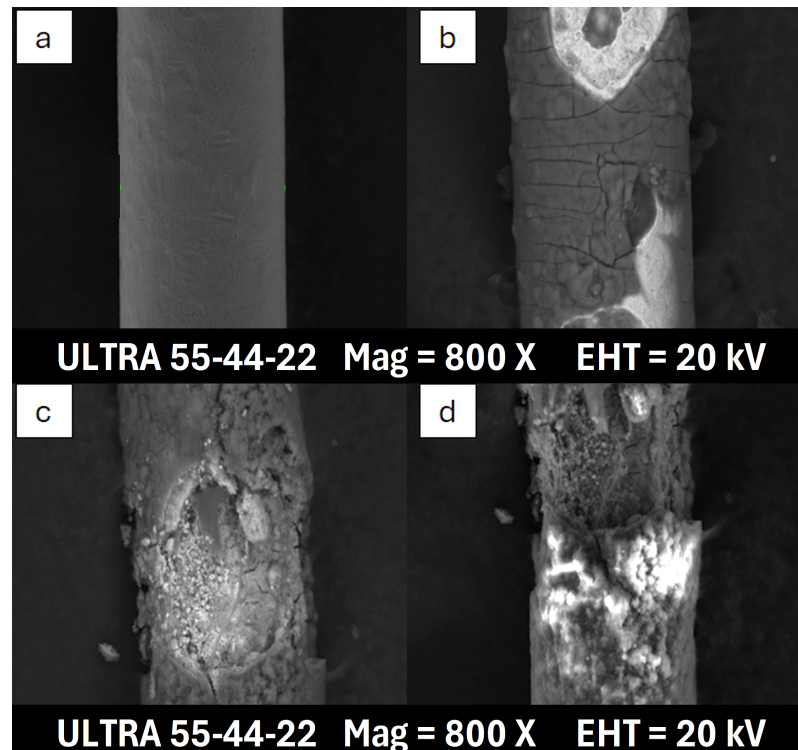


**Figure 12.** SEM images: (a) clean copper wire; (b) PAO\_VAP\_HP1; (c) DE\_VAP\_TB1; (d) PAO\_VAP\_TB2.

**Table 5.** Elemental analysis of the tested wires after immersion.

Heating Method	Fluid	State	Cu (%)	O (%)	C (%)	Other (%)
Heating plates 1	PAO	Clean wire	92.33	0.06	7.61	-
		OIL	65.45	6.71	27.69	0.15
		VAP	30.65	25.84	43.19	0.32
		OIL	67.49	6.38	25.95	0.18
		VAP	55.92	7.61	36.38	0.09
	DC	OIL	61.96	10.86	26.54	0.64
		VAP	66.98	4.18	28.84	-
	TR	OIL	67.74	6.94	25.21	0.09
		VAP	56.25	7.91	35.64	0.19
		OIL	69.18	6.55	23.99	0.27
		VAP	57.60	7.84	34.56	0.00
		OIL	64.97	8.49	26.25	0.29
		VAP	68.22	4.25	27.43	0.10

**Table 5.** Cont.

Heating Method	Fluid	State	Cu (%)	O (%)	C (%)	Other (%)
Thermal bath 1	PAO	OIL	72.91	4.09	22.83	0.17
		VAP	65.56	3.49	30.86	0.09
	DE	OIL	73.32	4.74	21.70	0.24
		VAP	34.86	20.16	44.68	0.30
	G-III	OIL	72.66	4.27	23.07	-
		VAP	60.13	6.40	33.39	0.08
Thermal bath 2	PAO	OIL	73.43	5.67	20.80	0.10
		VAP	39.58	18.38	41.92	0.12
	DE	OIL	70.80	4.89	24.31	-
		VAP	59.17	6.93	33.81	0.09
	G-III	OIL	73.24	4.08	22.67	0.01
		VAP	61.99	6.18	31.72	0.11

### 3.3. Copper Debris Quantification

It was found that all the fluids, except the dielectric coolant, had copper debris after the tests. A summary of the copper concentrations detected via the ICP measurements for all the tested fluids is presented in Table 6.

**Table 6.** Copper concentration (ppm) detected in the fluids tested via ICP measurements.

Method	Condition	TR	DC	PAO	G-III	DE
Heating plates 1	Fresh	n.d. <sup>1</sup>	n.d.	<1	-	-
	336 h	3.79	n.d.	4.92	-	-
Heating plates 2	Fresh	n.d.	n.d.	n.d.	-	-
	336 h	3.01	n.d.	1.51	-	-
Thermal bath 1	Fresh	-	-	n.d.	n.d.	n.d.
	336 h	-	-	1.03	1.83	3.67
Thermal bath 2	Fresh	-	-	n.d.	n.d.	n.d.
	336 h	-	-	1.37	1.52	<1

<sup>1</sup> Under detection limit.

Although in some cases the concentration of copper is higher than in others, it cannot be only attributed to copper corrosion because there are also connections of the DDM that may be in contact with the fluids. However, given that copper could not be detected below the detection limit in the dielectric coolant before or after the CWRCT, it can be inferred that it has a minimally corrosive effect on copper while immersed in the oil phase.

Nonetheless, notable variances in corrosion behavior among the fluids were found. Specifically, the vapor phase of PAO and the diester exhibited significant corrosion, as demonstrated by the increased resistance, the presence of corrosion byproducts after the immersion, and the elemental analysis showing copper oxide debris. Contrastingly, the dielectric coolant showed minimal corrosive effects on copper, as expected, implying superior compatibility as an e-thermal fluid for BEVs.

Finally, the advantages of this experimental approach include its sensitivity to detect slight changes in wire resistance and its provision of real-time insights into the corrosion process. However, the method's susceptibility to environmental factors like moisture and the need for precise control over experimental conditions presents challenges. Further research must be conducted to determine the viability of fluids as e-thermal fluids. Other factors such as thermal and electrical performance, costs, biodegradability, and sustainability have yet to be considered, and they could greatly influence its suitability.

## 4. Conclusions

This experimental methodology was proven to be sensitive for assessing resistance measurements of copper wires exposed to a corrosive fluid media. This sensitivity also

highlights the importance of controlling various experimental parameters, such as the wire length, connection methods, and ambient temperature, to ensure the reliability and reproducibility of the results. The influence of environmental factors, especially moisture, further complicates the corrosion dynamics, suggesting a significant impact of vapor conditions on the corrosion rate and pattern. Additionally, given that there were some signs of corrosion in all wires, future testing with thinner wires and/or longer test times could provide information about the rates of corrosion and further insights into the long-term behavior of e-thermal fluids in particular immersion environments.

Where there were higher resistance measurements, less copper and more oxygen were found on the surface, and an increase in copper concentration in the fluid was observed after the test, in addition to clear damage, which was shown in the SEM images.

Overall, resistance measurements, green droplets, SEM images with surface analysis, and the ICP analysis of the most affected wires were helpful in providing complementary evidence of copper corrosion and compatibility between the fluids and copper.

A notable variance in corrosion behavior among the tested fluids was effectively found. Some fluids showed exponential degradation patterns, while others demonstrated more linear trends. This variability emphasizes the complex nature of fluid–material interactions.

The dielectric coolant, which was formulated to be highly compatible with copper, emerged as the most suitable solution among the tested fluids. This is supported by the scanning electron microscopy (SEM) analysis, which revealed minimal damage to the copper wire exposed to this fluid, and the inductively coupled plasma (ICP) results, which showed no detectable copper debris. However, while copper compatibility is crucial, a comprehensive evaluation of e-thermal fluids necessitates a consideration of other factors such as thermal and electrical properties, cost, biodegradability, and sustainability.

Future research should focus on developing e-thermal fluids with enhanced thermal conductivity and specific heat capacity, along with excellent insulating properties. As coatings on copper wires serve as the first line of defense against corrosion, additional material compatibility tests should be conducted for plastics and elastomers commonly used in battery systems. These efforts will contribute to the advancement of immersion cooling technology, ensuring the optimal performance, longevity, and safety of battery electric vehicles.

**Author Contributions:** Conceptualization, B.T.; Methodology, S.R., J.A.-S. and L.I.F.-C.; Formal analysis, S.R.; Writing—original draft, J.A.-S.; Writing—review & editing, B.T. and L.I.F.-C.; Supervision, B.T. and L.I.F.-C. All authors have read and agreed to the published version of the manuscript.

**Funding:** This research was partly funded by project CIAICO/2021/013 from GVA, Generalitat Valenciana. The authors also want to acknowledge “Programa de Apoyo para la Investigación y Desarrollo” (PAID-01-22) for financing the PhD. studies of J. Alvis-Sánchez at Universitat Politècnica de València. L.I.F.-C. acknowledges the financial support given by Tecnológico de Monterrey within the challenge-based research project IJST070-23EG68001 (call 2023) to partially fund this research work.

**Data Availability Statement:** Data are contained within the article.

**Conflicts of Interest:** The authors declare no conflict of interest.

## References

1. International Energy Agency. Electric Car Sales Break New Records with Momentum Expected to Continue through 2023. 2023. Available online: <https://www.iea.org/reports/global-ev-outlook-2023/executive-summary> (accessed on 5 February 2024).
2. Kim, J.; Oh, J.; Lee, H. Review on battery thermal management system for electric vehicles. *Appl. Therm. Eng.* **2019**, *149*, 192–212. [[CrossRef](#)]
3. Pambudi, N.A.; Sarifudin, A.; Firdaus, R.A.; Ulfa, D.K.; Gandidi, I.M.; Romadhon, R. The immersion cooling technology: Current and future development in energy saving. *Alex. Eng. J.* **2022**, *61*, 9509–9527. [[CrossRef](#)]
4. Sundin, D.W.; Sponholtz, S. Thermal management of Li-ion batteries with single-phase liquid immersion cooling. *IEEE Open J. Veh. Technol.* **2020**, *1*, 82–92. [[CrossRef](#)]
5. Shell. Electric Vehicle Fluids. 2019. Available online: <https://www.shell.com/content/dam/shell/assets/en/business-functions/shell-lubricants/documents/shell-white-paper.pdf> (accessed on 6 February 2024).

6. *ASTMD130; Standard Test Method for Corrosiveness to Copper from Petroleum Products by Copper Strip Test.* ASTM International: West Conshohocken, PA, USA, 2019.
7. Hunt, G.J.; Gahagan, M.P.; Peplow, M.A. Wire resistance method for measuring the corrosion of copper by lubricating fluids. *Lubr. Sci.* **2017**, *29*, 279–290. [[CrossRef](#)]
8. Hunt, G.; Prengaman, C. *Understanding Vapor and Solution Phase Corrosion of Lubricants Used in Electrified Transmissions*; Technical Report, SAE Technical Paper; SAE International: Warrendale, PA, USA, 2020.
9. Hunt, G. *New Perspectives on Lubricant Additive Corrosion: Comparison of Methods and Metallurgy*; Technical Report, SAE Technical Paper; SAE International: Warrendale, PA, USA, 2018.
10. Wang, A.; Yin, X.; Xin, Z.; Cao, F.; Wu, Z.; Sundén, B.; Xiao, D. Performance optimization of electric vehicle battery thermal management based on the transcritical CO<sub>2</sub> system. *Energy* **2023**, *266*, 126455. [[CrossRef](#)]
11. Shrestha, S.; Baral, B.; Shah, M.; Chitrakar, S.; Shrestha, B.P. Measures to resolve range anxiety in electric vehicle users. *Int. J. Low-Carbon Technol.* **2022**, *17*, 1186–1206. [[CrossRef](#)]
12. Lacroix-Andrivet, O.; Hubert-Roux, M.; Loutelier Bourhis, C.; Moualdi, S.; Mendes Siqueira, A.L.; Afonso, C. Characterization of Base Oil and Additive Oxidation Products from Formulated Lubricant by Ultra-High Resolution Mass Spectrometry. *Lubricants* **2023**, *11*, 345. [[CrossRef](#)]
13. Soleimani, M.; Dehabadi, L.; Wilson, L.D.; Tabil, L.G. Antioxidants Classification and Applications in Lubricants. In *Tribology, Lubricants and Additives*; Johnson, D.W., Ed.; IntechOpen: Rijeka, Croatia, 2018; Chapter 2. [[CrossRef](#)]
14. Aromaa, J.; Kekkonen, M.; Mousapour, M.; Jokilaakso, A.; Lundström, M. The Oxidation of Copper in Air at Temperatures up to 100 °C. *Corros. Mater. Degrad.* **2021**, *2*, 625–640. [[CrossRef](#)]
15. Lee, S.K.; Hsu, H.C.; Tuan, W.H. Oxidation Behavior of Copper at a Temperature below 300 °C and the Methodology for Passivation. *Mater. Res.* **2016**, *19*, 51–56. [[CrossRef](#)]
16. De Carlo, I.; Baudino, L.; Klapetek, P.; Serrapede, M.; Michieletti, F.; De Leo, N.; Pirri, F.; Boarino, L.; Lamberti, A.; Milano, G. Electrical and Thermal Conductivities of Single Cu<sub>x</sub>O Nanowires. *Nanomaterials* **2023**, *13*, 2822. [[CrossRef](#)] [[PubMed](#)]
17. Peng, J.; Chen, B.; Wang, Z.; Guo, J.; Wu, B.; Hao, S.; Zheng, N. Surface coordination layer passivates oxidation of copper. *Nature* **2020**, *586*, 390–394. [[CrossRef](#)] [[PubMed](#)]
18. Young, H.D.; Freedman, R.A.; Ford, A.L.; Sears, F.W. *Sears and Zemansky's University Physics: With Modern Physics*, 13th ed.; Pearson Addison-Wesley: San Francisco, CA, USA, 2012.
19. Areny, R.P. Tetrapolar bioimpedance measurements compared to four-wire resistance measurements. *J. Electr. Bioimpedance* **2018**, *9*, 1–2. [[CrossRef](#)] [[PubMed](#)]
20. Ladino, L.; Rondón, S. Resistance of copper wire as a function of temperature. *Phys. Educ.* **2014**, *50*, 42. [[CrossRef](#)]
21. Sancarlos-González, A.; Pineda-Sánchez, M.; Puche-Panadero, R.; Sapena-Bano, A.; Riera-Guasp, M.; Martínez-Roman, J.; Pérez-Cruz, J.; Roger-Folch, J. Application of the parametric proper generalized decomposition to the frequency-dependent calculation of the impedance of an AC line with rectangular conductors. *Open Phys.* **2017**, *15*, 929–935. [[CrossRef](#)]
22. Młot, A.; Korkosz, M.; Grodzki, P.; Łukaniszyn, M. Analysis of the proximity and skin effects on copper loss in a stator core. *Arch. Electr. Eng.* **2014**, *63*, 211–225. [[CrossRef](#)]
23. Zheng, L.; Zheng, H.; Huo, D.; Wu, F.; Shao, L.; Zheng, P.; Jiang, Y.; Zheng, X.; Qiu, X.; Liu, Y.; et al. N-doped graphene-based copper nanocomposite with ultralow electrical resistivity and high thermal conductivity. *Sci. Rep.* **2018**, *8*, 9248. [[CrossRef](#)] [[PubMed](#)]
24. Abosede, O.O.; Obaleyé, J.A. New One-Pot Synthetic Route and Spectroscopic Characterization of Hydroxo-Bridged Stepped-Cubane Copper(II) Complexes. *Asian J. Appl. Sci. Technol.* **2022**, *6*, 21–31. [[CrossRef](#)]
25. Li, Y.; Fan, W.; Zhang, Z.; Xie, X.; Xiang, S.; Huang, D. Copper(II)-hydroxide facilitated C–C bond formation: The carboxamido pyridine system versus the methylimino pyridine system. *Dalton Trans.* **2020**, *49*, 12189–12196. [[CrossRef](#)] [[PubMed](#)]
26. Duvanova, E.; Mariichak, A.Y.; Baumer, V.; Rozantsev, G.M.; Radio, S.V. Crystal Structure if double sodium–Copper(II) Paratungstate B, Na<sub>2</sub>Cu<sub>4</sub>[W<sub>12</sub>O<sub>40</sub>(OH)<sub>2</sub>]·22H<sub>2</sub>O, and Mixed Copper (II) Paratungstate B–Hydroxode, Cu<sub>5</sub>[W<sub>12</sub>O<sub>40</sub>(OH)<sub>2</sub>]·2Cu(OH)<sub>2</sub>·30H<sub>2</sub>O. *J. Struct. Chem.* **2021**, *62*, 379–389. [[CrossRef](#)]
27. Saikova, S.; Vorob'ev, S.A.; Nikolaeva, R.; Mikhlin, Y. Conditions for the formation of copper nanoparticles by reduction of copper(II) ions with hydrazine hydrate solutions. *Russ. J. Gen. Chem.* **2010**, *80*, 1122–1127. [[CrossRef](#)]

**Disclaimer/Publisher's Note:** The statements, opinions and data contained in all publications are solely those of the individual author(s) and contributor(s) and not of MDPI and/or the editor(s). MDPI and/or the editor(s) disclaim responsibility for any injury to people or property resulting from any ideas, methods, instructions or products referred to in the content.